CZECH TECHNICAL UNIVERSITY IN PRAGUE
Faculty of Nuclear Sciences and Physical Engineering

Department of Physics

Study of multi-hit resolution and detector artefacts in silicon drift detectors

Diploma Thesis

Supervisor: Doc. RNDr. Vojtěch Petráček, CSc.

Jaroslav Adam

2009

Abstrakt
Název práce:
Studium mnohočásticového rozlišení a detektorových artefaktů v křemíkových driftových detektorech

Autor: Jaroslav Adam

Obor: Jaderné inženýrství

Druh prace: Diplomová práce

Vedoucí práce: Doc. RNDr. Vojtěch Petráček, CSc. Katedra fyziky, Fakulta jaderná a fyzikálně inzenýrská, České vysoké učení technické v Praze

Konzultant: —

Abstrakt:

Práce se ve své první části zabývá popisem struktury Vnitřního dráhového systému detektoru ALICE. Druhá část obsahuje vysvětlení principu křemíkového driftového detektoru a úvod k metodě pro numerický výpočet potenciálu elektrického pole v driftovém detektoru. Třetí část se zabývá vlastnostmi pohybu volných nosičů náboje v polovodiči. Jsou diskutovány efekty jako zejména drift nosičů náboje, difuze a vzájemná coulombická repulze. Čtvrtá část zahrnuje analýzu numerických metod pro simulaci transportu nosičů náboje v křemíkovém driftovém detektoru, jsou přiloženy ukázky simulací. Pátá část popisuje realizaci vyčítací elektroniky křemíkových driftových detektorů použitých v detektoru ALICE a zahrnuje popis metody pro simulaci zesilovací a kvantizační techniky. Šestá, poslední část obsahuje analýzu pohybu elektronů v detektoru s lokálně poškozeným potenciálem elektrického pole a důsledky na driftovou rychlost.

Klíčová slova: Polovodičové detektory, Driftový detektor, ALICE

Title:
Study of multi-hit resolution and detector artefacts in silicon drift detectors

Author: Jaroslav Adam

Abstract:

This project in the first part deals with description of the Inner Tracking System structure of the ALICE detector. The second part contains explanation of the principle of the Silicon Drift Detector and introduction to method for numerical calculation of the potential of the electric field in drift detector. The thirt part deals with basic characters of motion of free carriers in a semiconductors. Effects like carrier drift, diffusion and carriers mutual coulombic repulsion are discussed. The fourth part includes analyse of numerical methodes for simulation carrier transport in Silicon Drift Detector. Exemplary results of the simulations are attached. The fiveth part describes realization of the readout of the ALICE Silicon Drift Detectors and method for simulation of amplifying and quantization technics. The sixth, last part contains analyses of the electrons transport in drift detector with locally broken potential of the electric field and consequences to drift velocity.

Key words: Semiconductor detectors, Drift detector, ALICE

Prohlášení

Prohlašuji, že jsem svoji diplomovou práci vypracoval samostatně a použil jsem pouze podklady a zdroje (literatury, projekty, SW, atd.) uvedené v přiloženém seznamu.

Nemám žádný důvod proti užití tohoto školního díla ve smyslu §60 Zákona č. 121/2000 Sb., o právu autorském, o právech souvisejících s právem autorským a o změně některých zákonů (autorský zákon).

V Praze dne:

Podpis:

Acknowledgement

I would like to thank Doc. RNDr. Vojtěch Petráček, CSc. for his invaluable help, motivation, language and factual corrections throughout the preparation of this work.

Zadani prace

Contents

Chapter 1

Introduction

The aim of this project is to develope the slow detector simulator for ALICE Silicon Drift Detector system, which will allow simulation of the SDD functionality from the impact of the ionizing particle until the analog-digital conversion in readout electronics for single hits or simultaneous multi - hits in the drift or anode direction.

The produced simulator should serve as a source of data for the fast detector simulator in ALICE SDD software.

Chapter 2

Structure of the ITS

The Inner Tracking System of the ALICE detector is composed of the six layers of coordinate-sensitive detectors, which covers the central rapidity region ($|\eta| \leq 0.9$) and vertexes 10.6 cm along beam direction (z). The innermost layers with requirements of granularity are composed of the Silicon Pixel Detectors (SPD) and Silicon Drift Detectors (SDD) and for the third layer of ITS are used double sided Silicon Strip Detectors (SSD) with small stereo angle.

For connections from the frond-end electronics to the detector and to the readout are used TAP bonded aluminium multilayer microcables. Towards stabilization of the room temperature in the ITS is used a water cooling system.

2.1 The pixel layers

The two innermost layers are fundamental in determination of the position of the primary vertex, measurement of the impact parameter of secondary tracks from the weak decays of strange, charm and beauty particles. In the region of the pixel detectors the tracks density exceeds 50 tracks/cm^2.

The matrix of pixel detector contains 256×256 cells, each measuring 50 μm in the $r\phi$ direction and 300 μm in the z direction. Detector half - ladder has dimensions 13.8 mm ($r\phi$) $\times$ 82 mm (z). The detector is 150 μm thick and the electronic chip 100 μm thick, then total thickness of the detector is 250 μm.

Ladders are mounted into staves and this objects are built-up around the beam pipe to close the full barrel. Inner layer of SPD is located at an average distance of 4 cm and outer layer has average distance 7 cm (Fig. 2.1).

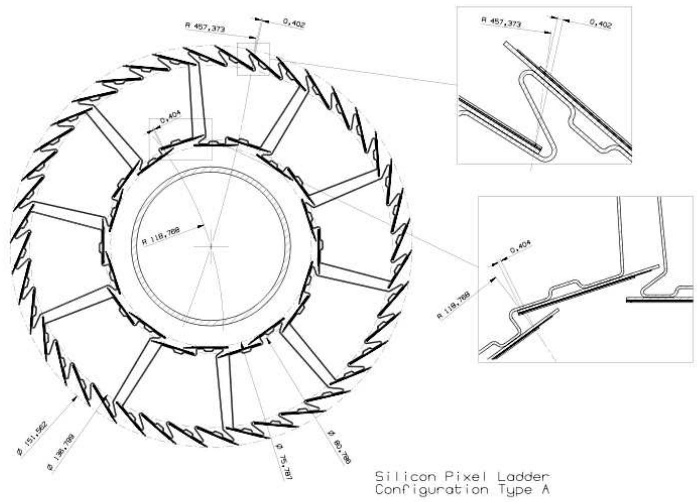

Figure 2.1: Section of the SPD layers [1].

2.2 The drift layers

The Silicon Drift Detectors fill two intermediate layers of ITS and provide in particular dE/dx information. Each SDD ladder holds six detectors for layer 3 and eight detectors for layer 4. Layers ocuppies average radius of 14.9 cm and 23.8 cm and are composed of 14 and 22 ladders respectively (Fig. 2.2).

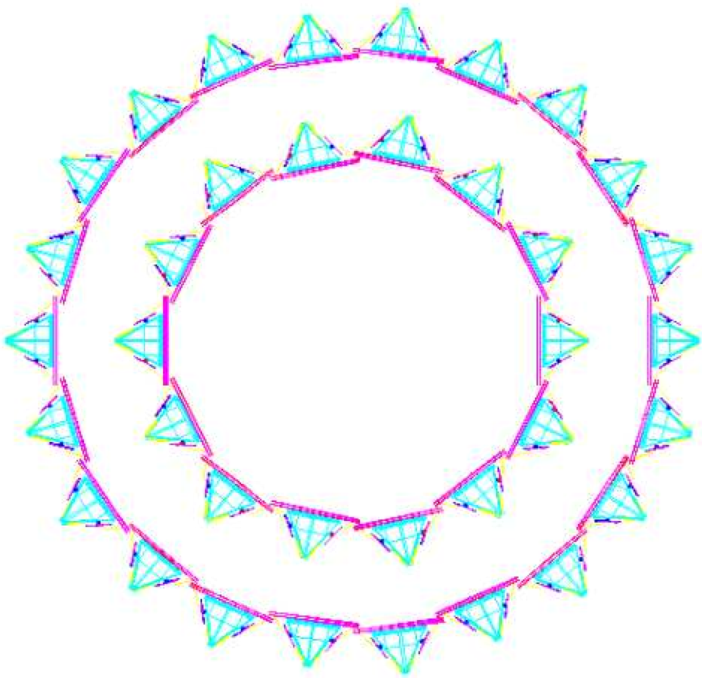

Figure 2.2: Section of the SDD layers [1].

2.2.1 The ALICE SDD final prototype

The final prototypes were produced on 300 μm thick 5" Neutron Transmutation Doped n-type wafers with a resistitity of 3 kΩ cm. The active area of the detector is 7.02×7.53 cm^2, and the total detector area is 7.25×8.76 cm^2, whence the ratio the active area to the total area is 0.85 (Fig. 2.3). The active area is parted into two opposite 35 mm long drift regions, each equipped with 256 collecting anodes of 294 μm pith. Both the drift and the guard sides dispose of integrated voltage dividers. The monitoring of the drift velocity performs three rows 33 implanted point-like MOS charge injectors.

Designed two tracks resolution in $r\phi$ direction is 200 μm and 600 μm in the z direction.

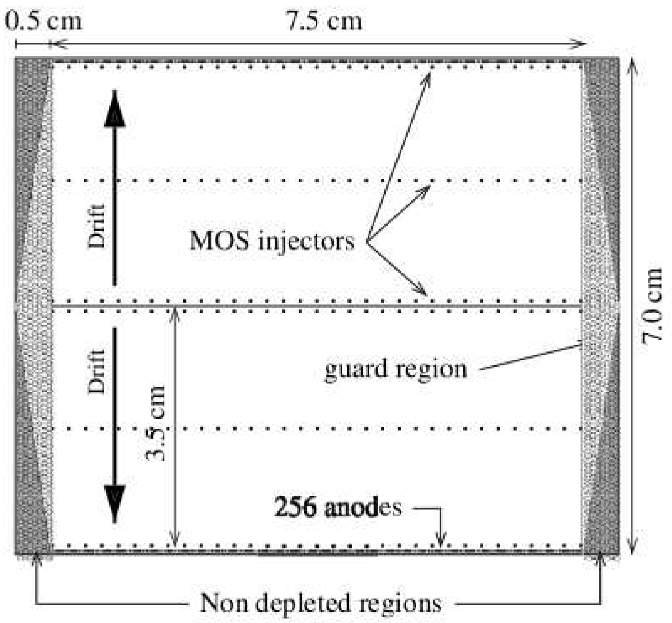

Figure 2.3: Sketch ALICE SDD final prototype [2].

2.3 The strip layers

The two outer layers of the ITS also provides dE/dx information and are crucial for the connection of tracks from the ITS to the Time Projection Chamber (TPC). Stereo angle of this double sided SSDs is 35 mrad and each detector has total area of 75 mm by 42 mm (fig. 2.4). The strips of the SSDs are mounted (nearly) parallel to the magnetic field. The Silicon Strip Detectors are made on n-type silicon wafers with thickness of 300 μm.

Each strip is 40 mm long and tilted by an angle of 17.5 mrad with respect to the short side of the detector. The implantation of strips is taken by p^+ doping on the junction side and n^+ doping on the ohmic side. The active area of the detector is surrounded by guardings to separate the active area from damaged silicon structure at the cut edges of the detector. The bias and guard structures covers 1 mm wide areas on all sides of the detector leaving an active area of 40 $\times$ 73 mm^2. Separation of the leakage currents in the strips from the inputs of the readout electronics is provided by the integrated capacitors on top of each strip.

The minimum-ionizing particle crosses the depleted detector normally to its major surfaces leaves a charge of about 25 000 electrons. The resolution is better then the geometric resolution ($\sim$ 30 μm) for mips arriving normally

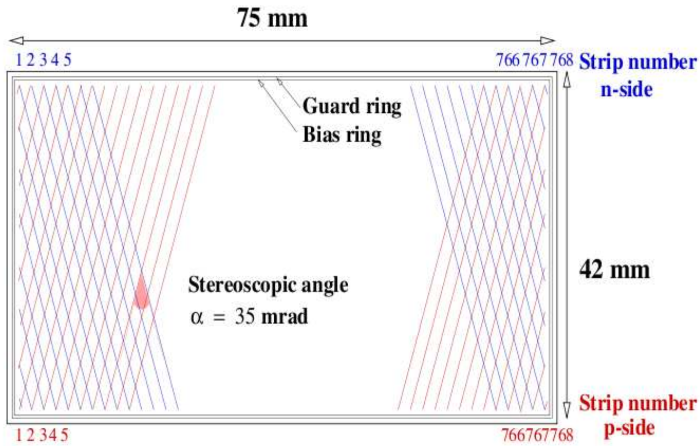

Figure 2.4: Scheme of part of SSD [1].

at the detector.

Chapter 3

Principle of the Silicon Drift Detector

The main feature of this detector is that electrons are transported parallel to large surfaces of the detector onto a small area n^+ anode connected to the input of an amplifier, while holes from an ionization created electron-holes pairs are transported to the nearest p^+ cathode. The principle of detector is schematically shown in Fig. 3.1. [1]

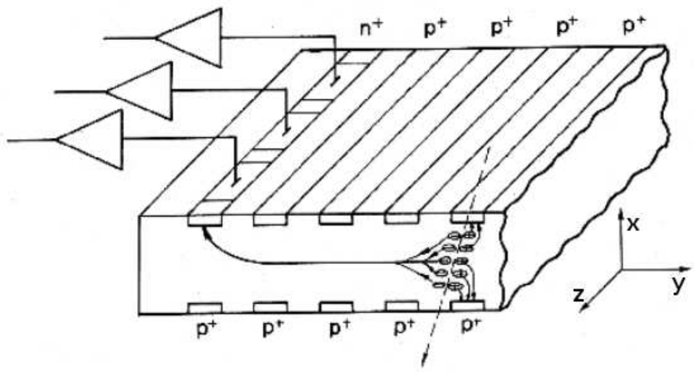

Figure 3.1: Principle of semiconductor drift detector [3], [1].

Position sensitivity in the drift direction is maintained by measurement of the drift time of the electrons and position sensitivity in the anode direction is determined by 294 μm anode pith.

The capacitance of anode in ALICE SDD (4 fF) is very small, practically

[1]Figure 3.1 shows so-called linear silicon drift detector, but also exist the cylindrical silicon drift detectors.

independent of the detector size and decreases the effect of the preamplifier series noise.

The electric field responsible for the electron transport inside the detector is given by the Poisson's equation, which is formulated for the negative potential, [3]:

$$\frac{\partial^2(-\phi)}{\partial^2 x} + \frac{\partial^2(-\phi)}{\partial^2 y} = \frac{N_D q}{\epsilon_0 \epsilon_r}, \tag{3.1}$$

where N_D is the density of ionized donors in silicon bulk, ϵ_r is relative dielectric constant, ϵ_0 is permeability and q is (positive) electronic charge.

The potential is independent of the z-coordinate (Fig. 3.1) along the p^+n junction and the detector (n-type silicon) is fully depleted of free carriers. Realization of the potential is provided by applying appropriate voltages to the linear array of rectyfying p^+n junctions and in the ALICE SDD these voltages are determined by the integrated voltage divider (Fig. 3.2)

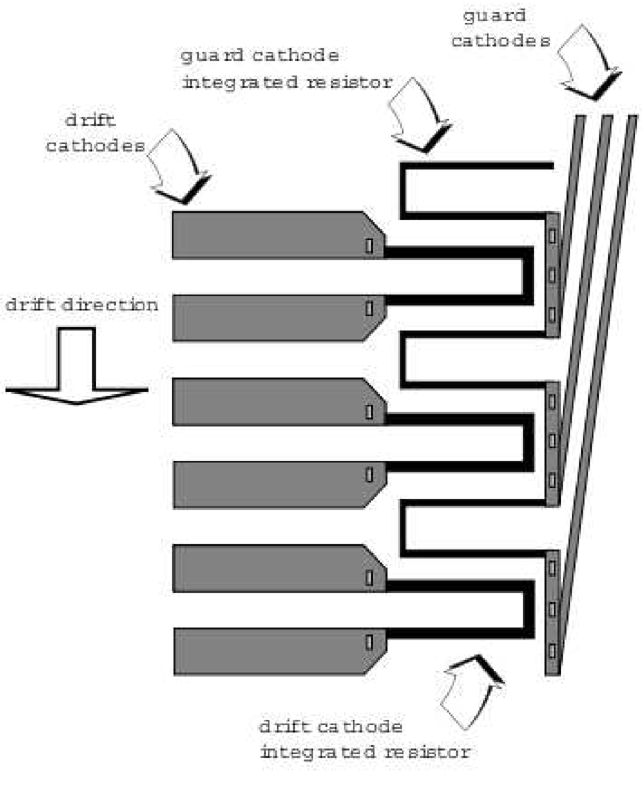

Figure 3.2: Integrated voltage divider (ALICE Silicon Drift Detector) [1].

The surface of the detector between two adjacent drift cathodes is covered by thermally grown SiO_2. The boundary conditions on Si-SiO_2 are defined by net positive charges in the oxide.

After creation the electrons by fast particle crossing the detector this electrons are focused by the field into the center plane of the detector and transported in this plane towards the anode. The focusation process is shown in Fig. 3.3.

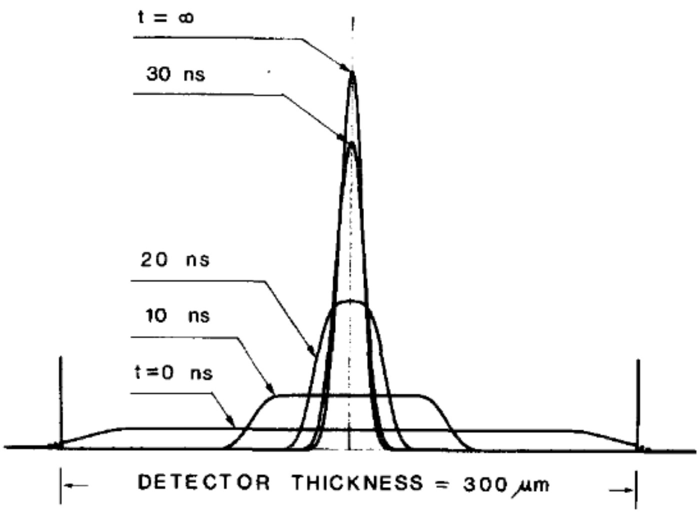

Figure 3.3: Electron distribution along the detector tepth for initial uniform distribution at different elapsed times [4].

The drift time of electrons created by ionizing particle is measured as the delay of siglal induced on the detector anode by a cloud of arriving electrons relative to the crossing time of the particle. The electrons drift time is proportional to the distance between anode and crossing point of the ionizing particle. In the region close to the anode the potencial of the electric field has a different shape, the minimum of the electron potential energy is shifted from the central plane of the detector toward the anode side of the detector.

3.1 Numerical calculation of the potential of the electric field in the SDD

For numerical calculation of the potential has been used program named *Posibin* [3], written in FORTRAN 77, which numerically solves Poissons equation (3.1) for potential ϕ. Input of the *Posibin* is ascii file containing information about positions and dimensions of p^+ cathodes and the respective voltages. As output is created another ascii file with information of potentials on the net of 129 × 181 points covering simulated area. Included are also distances between neighbouring net points in microns.

Potential in the linear part of the ALICE Silicon Drift Detector is shown on the Fig. 3.4, in the anode part of detector on Fig. 3.5.

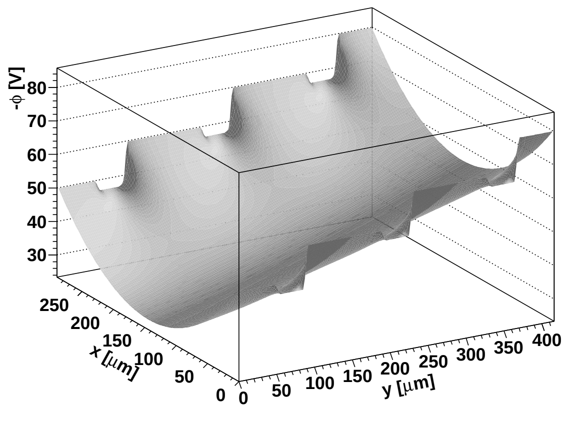

Figure 3.4: Potential of the electric field in linear part of the ALICE SDD.

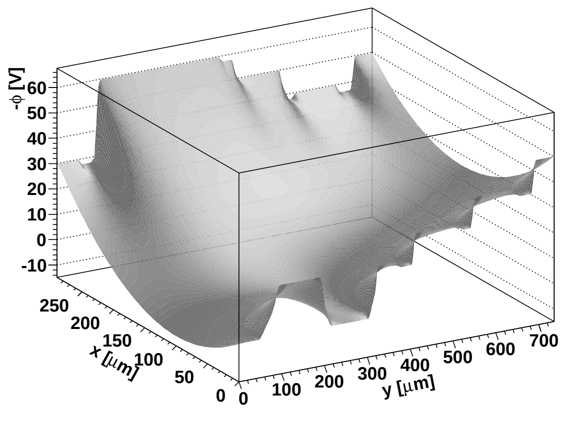

Figure 3.5: Potential of the electric field in anode part of the ALICE SDD.

From the previous figures 3.4 and 3.5 is evident, that maximum distances in drift direction (y) allowed by *posibin* are small with comparison to the dimensions of the detector (drift region 35 mm long in ALICE SDD), consequently the *posibin* output files must be connected to each other. Connection between anode part and first linear part of the ALICE Silicon Drift Detector can be seen on the Fig. 3.6, in the equipotential representation on the figure (3.7). Addition of the linear parts can be performed several times, with correct posibin input file.

The connection of the *posibin* output files with 129 $\times$ 181 net of potentials in xy axes demands the continuity in the values of potential and first derivatives of the potential with respect to the drift direction y. The continuity in the values at neighboring points of the adjoininig files is ensured by correct *posibin* input files, but the continuity in the first derivatives must be introduced by the cubical parabola (3.2) interpolation of the end and start regions of two adjacent output files.

$$V = c_1\frac{y^3}{3} + c_2\frac{y^2}{2} + c_3 y + c_4. \tag{3.2}$$

Interpolation is taken between 6 last points and 8 first points of previous and following file, which is for dy = 2.7 μm distance about 16.2 μm and 21.6 μm respective. Coeffitients c_1 - c_4 of the cubical parabola are calculated from the values and the first derivatives at the start (y_1) and end (y_2) points of the each cubical parabola. This requirements forms the matrix equation (3.3) with unknow c_1 - c_4:

$$\begin{pmatrix} y_1^2 & y_1 & 1 & 0 \\ y_2^2 & y_2 & 1 & 0 \\ \frac{y_1^3}{3} & \frac{y_1^2}{2} & y_1 & 1 \\ \frac{y_2^3}{3} & \frac{y_2^2}{2} & y_2 & 1 \end{pmatrix} \begin{pmatrix} c_1 \\ c_2 \\ c_3 \\ c_4 \end{pmatrix} = \begin{pmatrix} V'(y_1) \\ V'(y_2) \\ V(y_1) \\ V(y_2) \end{pmatrix}. \tag{3.3}$$

This matrix equation is solved by the LU decomposition implemented it standard linear algebra library *lapack*.

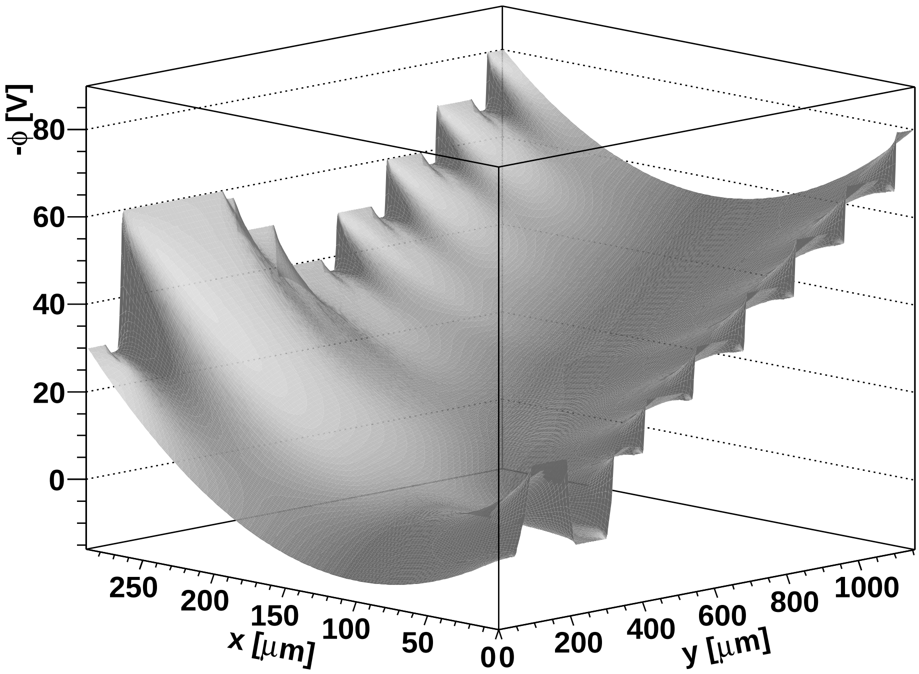

Figure 3.6: Potential of the electric field in anode and adjacent linear part of the ALICE SDD.

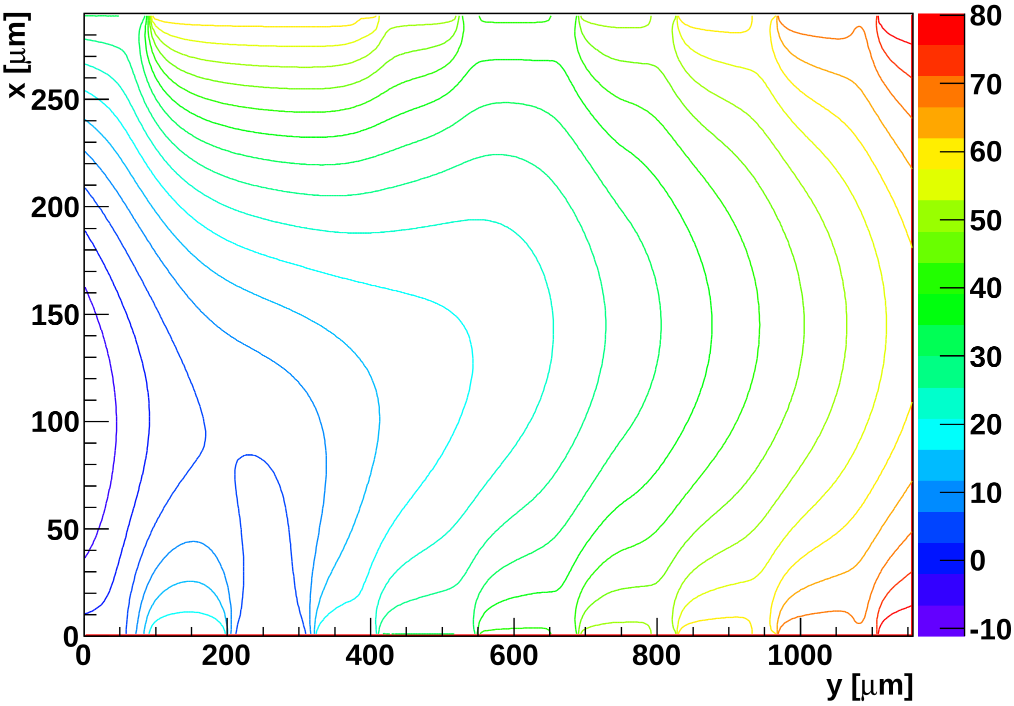

Figure 3.7: Potential of the electric field in anode and adjacent linear part of the ALICE SDD in the equipotential representation.

Chapter 4

Carrier transport in semiconductors

Motion of free carriers can be caused by application of an external electric field, this mechanism is reffered as carrier drift. In addition, carriers also move from regions with high carrier density to the regions with lower carrier density. This mechanism is carrier diffusion and is due to thermal energy. The total current in a semiconductor equals the sum of the drift and diffusion current.

After application an electric field to a semiconductor, the carriers accelerates and reach a constant average velocity v, at high applied field at saturation velocity v_{sat}. The carrier mobility μ is defined as the ratio of the velocity to the applied field. The electrons and the holes mobilities are quite different and depends on the doping density, as is shown on the Fig. 4.1.

Dependence of the carriers velocity on the electric field with taking account the saturation velocity is given by the following equation (4.1): graphically it is shown on the figure 4.2.

$$v = \frac{\mu E}{1 + \frac{\mu E}{v_{sat}}}. \tag{4.1}$$

Electric field has dimension of Vcm^{-1}, dimension of the mobility is cm^2/(V.s), so that the dimesion of the velocity in equation (4.1) is cm/s. This equation (4.1) holds for materials without accessible higher bands (e.q. sillicon) and their graphical representation is on the figure (4.2).

For describing the diffusion effects is useful to define the diffusion constant D_n as a product of a thermal velocity and the mean free path. Then the diffusion current J_n will be given as

$$J_n = qD_n \frac{\mathrm{d}n}{\mathrm{d}x}, \tag{4.2}$$

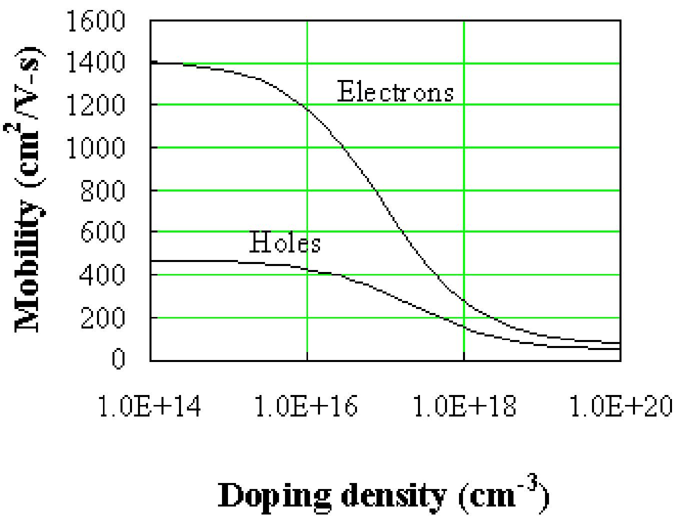

Figure 4.1: Mobility of the electrons and the holes [5].

where q is the unit charge and $n(x)$ the carrier density.

Relation between the diffusion constant and the mobility expresses Einstein relation:

$$D_n = \mu_n \frac{kT}{q} = \mu_n V_t, \tag{4.3}$$

where kT is thermal energy, V_t is thermal potential and n represents electrons or holes.

The total current of the free carriers in the semiconductor is obtained by adding the current due to diffusion to the drift current:

$$J_n = qn\mu_n E + qD_n \frac{\mathrm{d}n}{\mathrm{d}x}. \tag{4.4}$$

Besides the drift and diffusion effects is for cloud of the drifting carriers also important the mutual coulombic repulsion. The potential of this repulsion ϕ_j acting to the j-th carrier of the clout consisting of the N carriers is given by the formula (e is the positive unit charge in coulombs):

$$\phi_j = \sum_{i=1, i\neq j}^{N} \frac{1}{4\pi\epsilon_0\epsilon_r} \frac{e}{r_{ij}}. \tag{4.5}$$

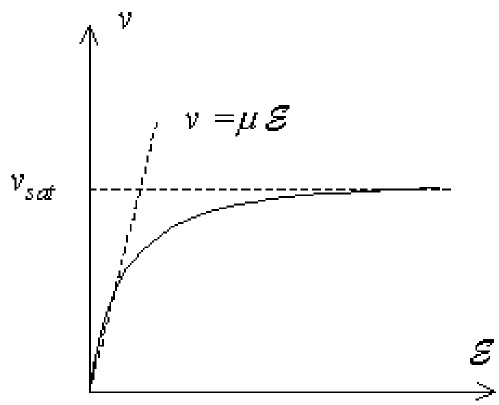

Figure 4.2: Dependence of drift velocity on electric field for materials without accessible higher bands (e.g. silicon) [5].

Chapter 5

Simulation of the carrier transport in the ALICE Silicon Drift Detector

Suppose that electrons and holes are created in detector with uniform distribution along the crossing line of the ionizing particle. For pions in the momentum range 290 - 310 MeV/c it obtains 19 000 electron-hole pairs, in the case of impact the proton with momentum in momentum interval 190 - 200 MeV/c is created 590 000 electron-hole pairs [1].

The purpose of the simulation is to find trajectories of all electrons from their creation to their arrival into anode and show their time distribution, which leds to the analog pulse qua an input for the preamplifier.

It is necessary to numerically solve equation (4.1) for the drift, with taking account the mutual coulombic repulsion (4.5) and the diffusion effect. In directions x and y (Fig. 3.1) is the potential of the electric field given by drift cathodes and mutual coulombic repulsion of the drifting charge cloud, in the z direction the potential has pure coulombic character.

Such numerical calculation performs the program *alidrift* written in Fortran 90, which solves equation (4.1) in all 3 space dimensions by the Runge-Kutta method, [6]:

$$
\begin{aligned}
k_1 &= \mathrm{d}t f_1(x_n, y_n, z_n) \\
l_1 &= \mathrm{d}t f_2(x_n, y_n, z_n) \\
m_1 &= \mathrm{d}t f_3(x_n, y_n, z_n) \\
k_2 &= \mathrm{d}t f_1(x_n + \frac{1}{2}k_1, y_n + \frac{1}{2}l_1, z_n + \frac{1}{2}m_1) \\
l_2 &= \mathrm{d}t f_1(x_n + \frac{1}{2}k_1, y_n + \frac{1}{2}l_1, z_n + \frac{1}{2}m_1) \\
m_2 &= \mathrm{d}t f_1(x_n + \frac{1}{2}k_1, y_n + \frac{1}{2}l_1, z_n + \frac{1}{2}m_1) \\
x_{n+1} &= x_n + k_2 \\
y_{n+1} &= y_n + l_2 \\
z_{n+1} &= z_n + l_3 \\
t_{n+1} &= t_n + \mathrm{d}t
\end{aligned}
\tag{5.1}
$$

Functions f_1, f_2 and f_3 are the right side of the equation (4.1) relevant for the x, y and z axes, t is a time variable and $\mathrm{d}t$ denotes the time step of the simulation. In all presented simulations has been used time step $\mathrm{d}t =$ 0.1 ns. The potential of the electric field created in the detector by the drift cathodes is calculated by *posibin*, connection of the *posibin* output files is taken by *alidrift* (singe *posibin* output file contains a net of 129×181 points with information of the potential and covers very small area with respect to the dimensions of the detector). Potential of the coulombic repulsion is calculated directly from the formula (4.5) and in the x (detector thickness) and y (drift direction) directions is the total electric field in equation (4.1) given as a sum of the field created by the drift cathodes and the coulombic field, in the z direction is electric field only coulombical (equation (4.5)).

Diffusion is superimposed as the random movement in the scale of the diffusion velocity (diffusion constant D_n mentioned in equation (4.3) is a product of the thermal velocity and the mean free path). In program *alidrift* is diffusion movement calculated via diffusion velocity. For each drifting carrier is in diffusion subroutine calculated distance covered by the respective carrier between the actual and previons Runge-Kutta step and diffusion constant D_n is divided by this distance to obtain diffusion velocity relevant for actual step of the Runge-Kutta method. Finally is relevant diffusion velocity multiplied by the random vector $\vec{r}$, which all three components contains pseudorandom numbers with values from -1 to 1 of uniform distribution. Contribution of the diffusion movement for all coordinates is calculated as multiplying respective diffusion velocity components by the time step $\mathrm{d}t$ of the Runge-Kutta method.

For including the discrete net of the potentials calculated by *posibin* to the simulation is essential to interpolate each rectangle generated of the directly neighboring points by a plane with equation

$$V(x, y) = a(x - x_0) + b(y - y_0) + c, \tag{5.2}$$

where x_0 and y_0 are coordinates of the middle of the rectangle. Interpolation is accomplished by the method of the least squares and minimization is performed by the simplex method [6], [7].

Considering the one step in Runge - Kutta method (5.1) must be taken for the each carrier (electron and hole) and calculation of the coulombic repulsion potential (4.5) goes over all carriers, the complexity of the *alidrift* algorithm is $O(N^2)$. Fortunately, the holes drifts to the nearest drift cathode and disappears after several decades of nanoseconds, but calculation time is still slightly high. On this account is suitable approximation, whereby one space point can contains several electrons or holes. The total number of the drifting electrons is decomposed to the number of the space points for the simulation and the number of the electrons at single point.

At start of the simulation, the electron – holes pairs are created with uniform distribution along whole detector thickness on the line with arbitrary elevation and slope. Mobility of the electrons is taken as 140 μm^2/V.ns, value of holes mobility is 40 μm^2/V.ns and saturation velocity parameter v_{sat} has been used as a calibration parameter for drift velocity 8.77 μm/ns pertinent to the drift field 714 V/cm.

Output of the *alidrift* program are ascii files carrying information of the electron and holes trajectories (recorded are all space points for all time steps of the simulation) and the time behaviour of the electric current inducated in the anode (anodes) by the arriving electrons. Trajectories points are in dimensions of μm, current in the anode in nano ampers nA. For displaying electron distribution on different anodes are also recorded arriving times and anode numbers relevant for all electrons.

Three - dimensional visualization of trajectories of the 100 electrons drifting from 2700 μm above detector anode edge is on the Fig. 5.1, 20 000 electrons on the Fig. 5.2 and 100 000 electrons drifting from 2640 μm above detector anode edge with slope of the initial distribution line of 0.4 on the Fig. 5.3. The drift direction is the opposite direction to the y axis, x axis is the detector thickness. Number 20 000 has been decomposed into 1000 space points and 20 electrons in one point, number 100 000 into 1000 space points and 100 electrons in single point.

The two - dimensional projections to xy axes of the previous 3D trajectories with equipotentials of the drift electrical field (100, 20 000 and 100 000

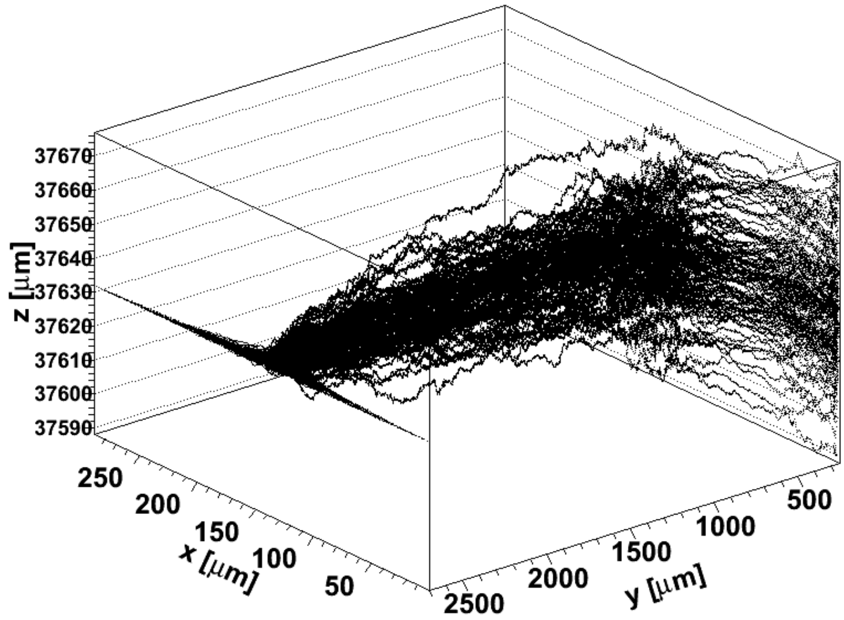

Figure 5.1: 3D visualization of the paths of the 100 electrons in SDD

electrons drifting from 2700 μm above detector anode edge) are shown on the figures 5.4, 5.5 and 5.6.

The time behaviour of the current inducated on the anode by the 20 000 and 100 000 electrons drifting from 2700 μm above detector anode edge is illustrated on figures 5.7 and 5.8.

If there are created two initial electron-holes distributions with different z coordinate, the electron trajectories have the following shape (Fig. 5.9) and the distribution of arrival electrons in different anodes is displayed on the figure 5.10.

Creation and drift trajectories of the two initial distributions of the electron-holes pairs with different y coordinate (different distance in the drift direction) is illustrated on the figure 5.11 and respective current in the anode on the figure 5.12. Each initial distribution contains 20 000 electrons, first starts from $y = 2000$ μm and second starts from $y = 2500$ μm and both are created in the same time.

When is demanded the simulation over larger drift distances is inevitable to take extrapolation of the electrons distribution from place of the detector relatively far from anodes to the region of the linear part of the detector close

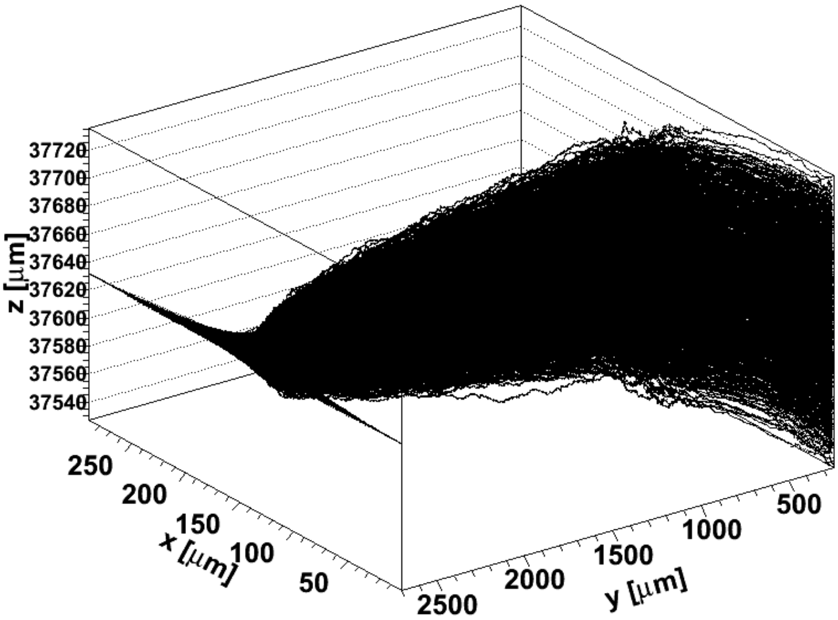

Figure 5.2: 3D visualization of the paths of the 20 000 electrons in SDD

to the anode.

In the steady state of the drift, between the position 60 ns after creation electron-holes pairs and the anode region, the electrons space distribution can be described by the gaussians for each axis respective.

$$n(x) = \frac{1}{\sqrt{2\pi\sigma^2}} e^{-\frac{(x-a)^2}{2\sigma^2}} \tag{5.3}$$

Mean a and variance σ for each axis are calculated directly from position distribution of electrons and stored in the dynamic array. Then there are six gaussian parameters (two for each axis), which must be linear interpolated with respect to time. Optimal distance for collecting the gaussian parameters is $> 800\ \mu$m. Linear interpolation is taken by the least squares method and for minimization is used the simplex method [6], [7].

After reaching start of the extrapolation distance, the time dependence of the gaussian parameters is given by the linear time dependence obtained by the previous interpolation. At the end of the extrapolation distance the electrons position distribution is generated from extrapolated gaussian parameters by the Box-Muller method ([6], [7]) and simulation continues by the previous way (numerial solving of the equation 4.1).

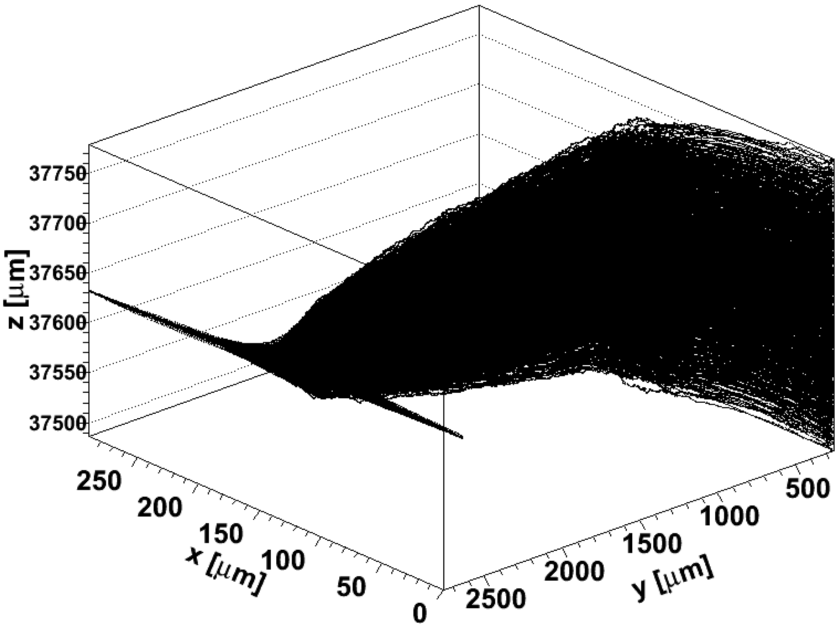

Figure 5.3: 3D visualization of the paths of the 100 000 electrons in SDD

The slope of the linear time dependence of the mean a in the y axis is directly the drift velocity, extrapolation can be performed multiply within one simulation at the different parts of the detector.

Double extrapolation of 1000 electrons drifting from $y = 7500$ μm with first extrapolation from $y = 6100$ μm to $y = 4600$ μm and second extrapolation from $y = 2500$ μm to $y = 1500$ μm is shown on the figure 5.13. Inside the extrapolation distance is for orientation generated actual xyz gaussians.

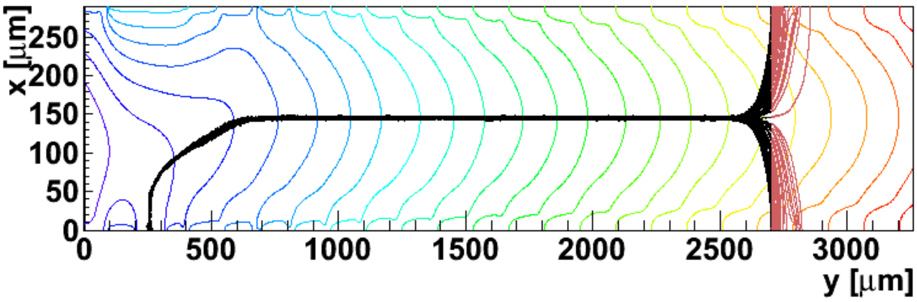

Figure 5.4: 2D projection of the paths of the 100 electrons (black) and holes (red) in SDD with equipotentials of the drift electric field

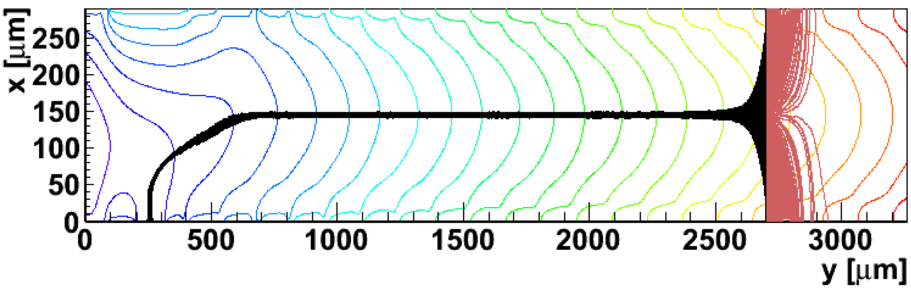

Figure 5.5: 2D projection of the paths of the 20 000 electrons (black) and holes (red) in SDD with equipotentials of the drift electric field

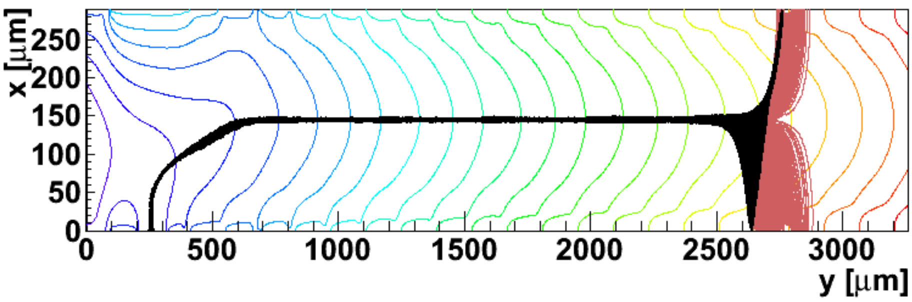

Figure 5.6: 2D projection of the paths of the 100 000 electrons (black) and holes (red) in SDD with equipotentials of the drift electric field

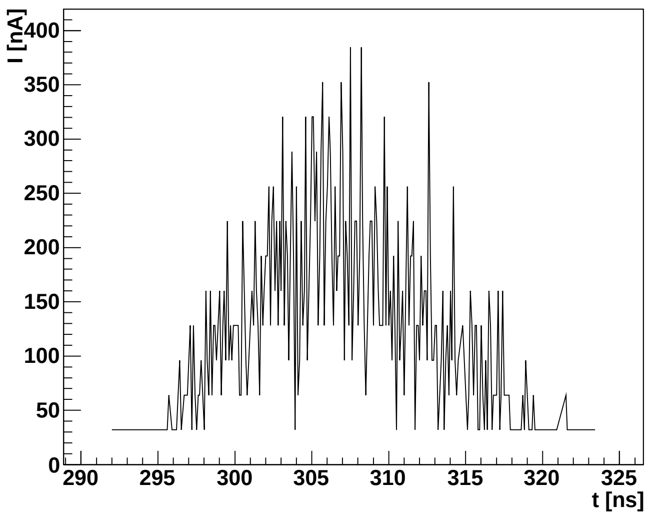

Figure 5.7: Current generated in the SDD anode by the 20 000 electrons drifting from distance of 2700 μm above the detector anode edge

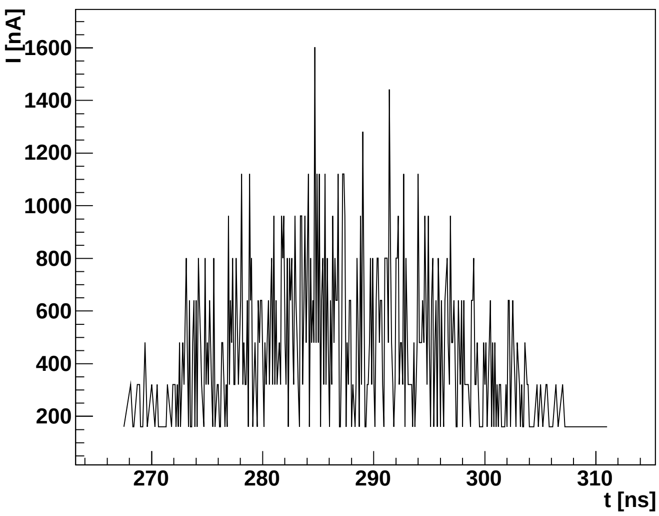

Figure 5.8: Current generated in the SDD anode by the 100 000 electrons drifting from distance of 2700 μm above the detector anode edge

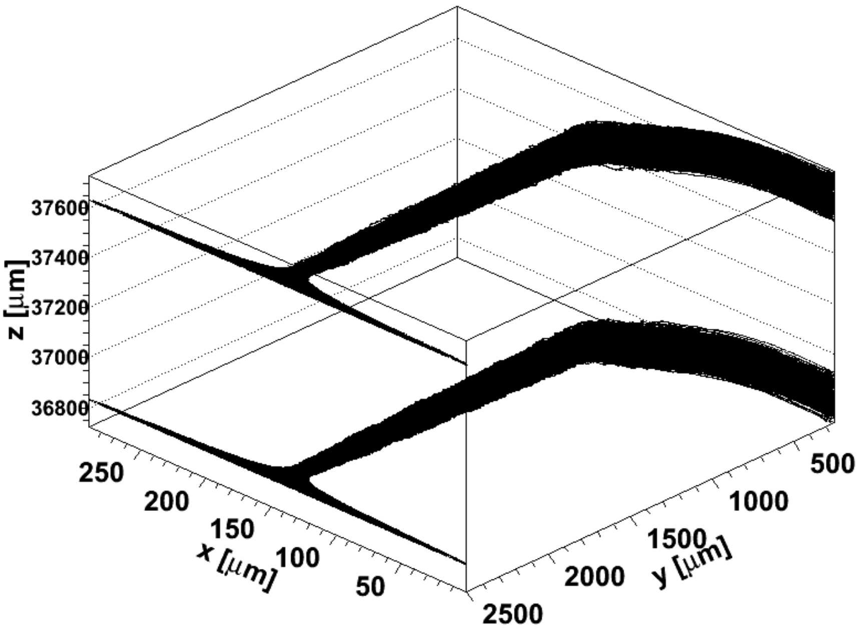

Figure 5.9: Trajectories of the 20 000 electrons initially distributed in $y =$ 2500 μm at the same time with mutual z distance of 800 μm.

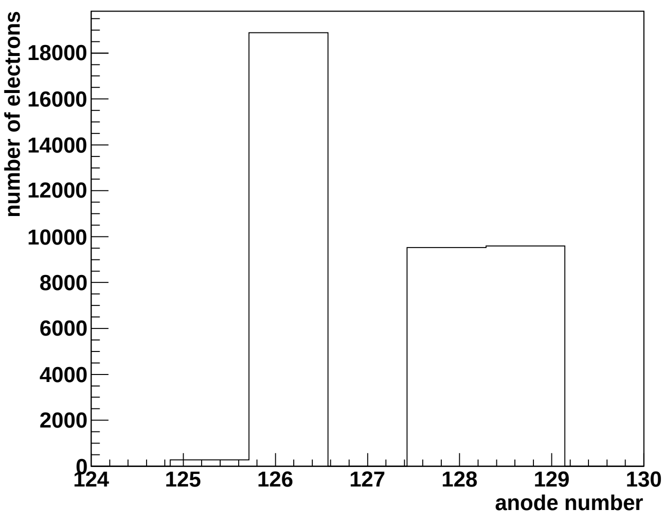

Figure 5.10: Anode distribution of the 20 000 electrons initially distributed in $y = 2500$ μm at the same time with mutual z distance of 800 μm.

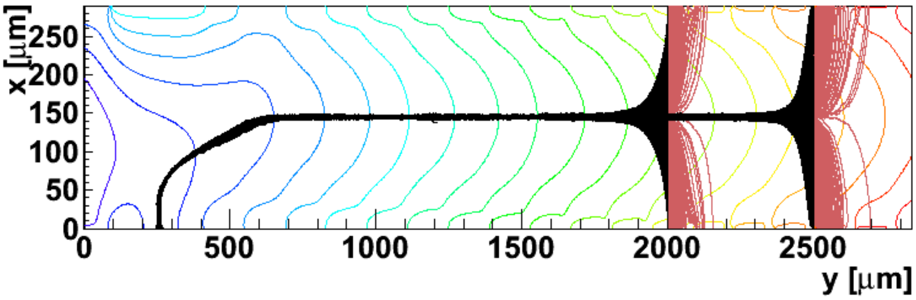

Figure 5.11: 2D visulalization of the two initial 20 000 electron-holes distributions.

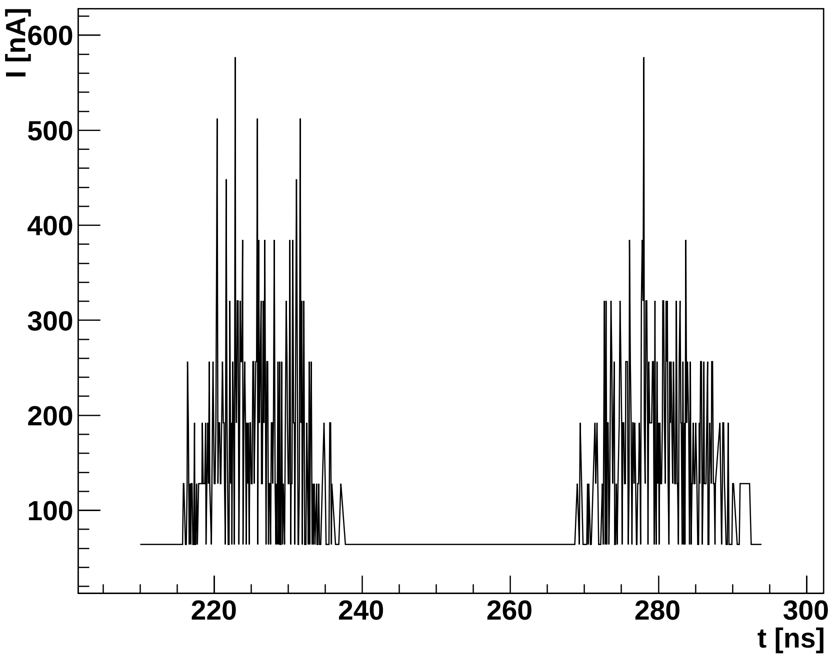

Figure 5.12: Current inducated in the anode by the two initial 20 000 electron-holes distributions created at the same time.

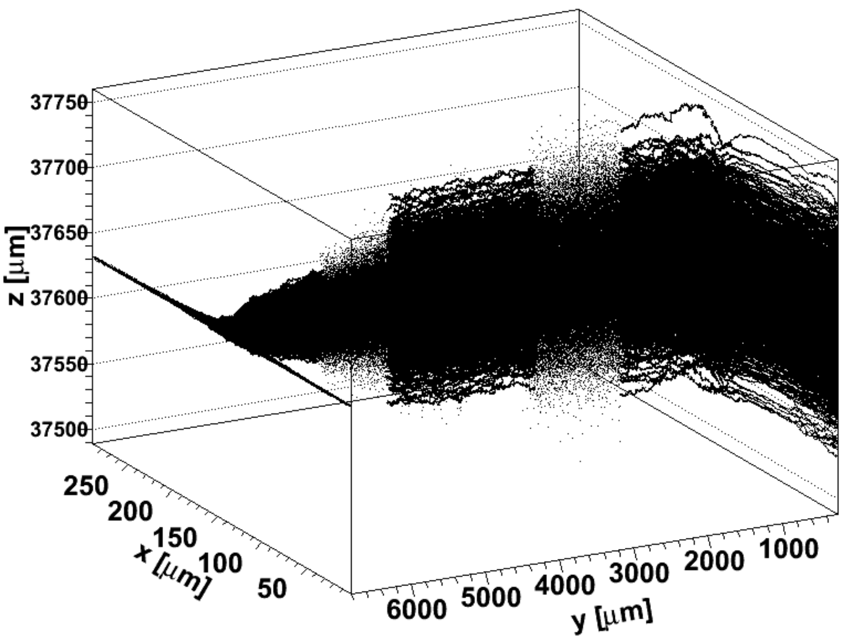

Figure 5.13: Double gaussian extrapolation in the y axis.

Chapter 6

SDD readout

The front end unit is shown in Fig. 6.1, consists of a hybrid circuit containing four submodules of the preamplification, analog storage and ADC architecture (called PASCAL) and multi-event buffer (called AMBRA) integrated circuit pair. The data transmition of the whole SDD barrel is subdivided into half ladders, the total readout time of the SDD should be lower then 1 ms. The readout of the ladder of the third layer is shown as a block diagram in Fig. 6.2. For read out a half SDD four pairs of chips are needed.

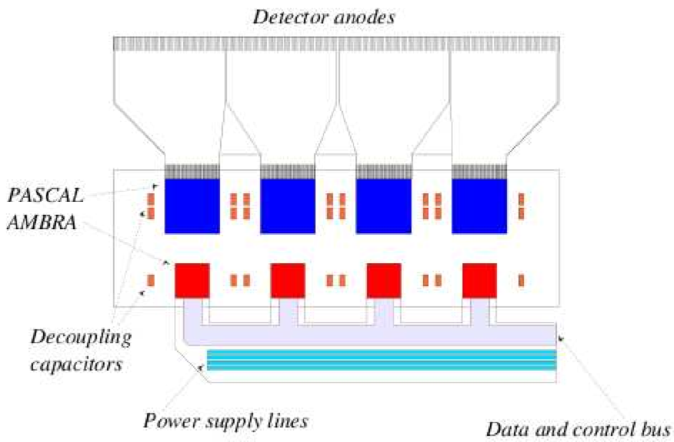

Figure 6.1: The front-end readout unit [1].

Hybrid circuit PASCAL provides both the preamplification and the digitalization with a dynamic range of 32 fC. The preamplifier has been designed to have an equivalent noise charge (ENC) of 250 e^- for zero anode capacitance and the A/D converter to have 10-bit precision. The ratio of the highnest signals (200 000 e^-) to the noise (250 e^-) is 800. Dynamic range

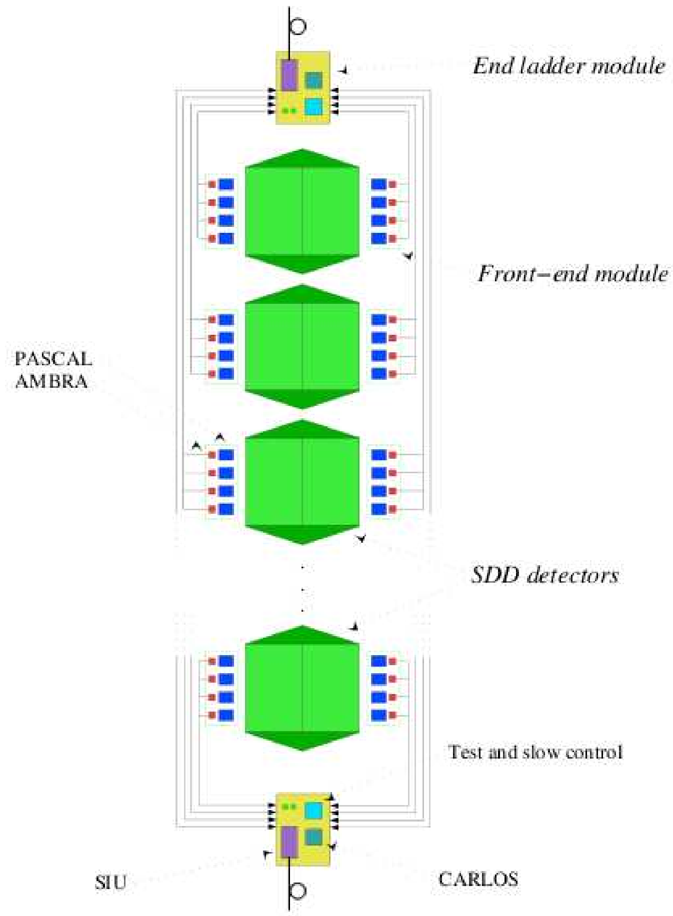

Figure 6.2: The SDD readout architecture [1].

for the input signal of the prepmplifier is 0.04 - 32 fC, maximal signal charge is 160 fC and the gain for a δ-like pulse is 27 mV/fC [8]. The linearity of the preamplifier for the negative and positive output and for the 50 Ω load and the 1MΩ load is shown in the Figure 6.3.

The sapmling frequency for the SDD signal is 40 MHz, the same of the clock frequency of LHC. The preamplifier peaking time is 40 ns. A/D converter operated at 40 Msample/s should unacceptable power consumption. Therefore PASCAL contains an intermediate, 256 channel, analogue ring memory for each channel which samples the output of the preamplifier every 25 ns. After receiving a trigger the contents of the analogue memories are frozen and read out by the ADCs with a conversion rate of 2 Msample/s. The total readout time is about 250 μs.

The gain of the ADC for pulse generated by 1 MIP is 110 ADC counts,

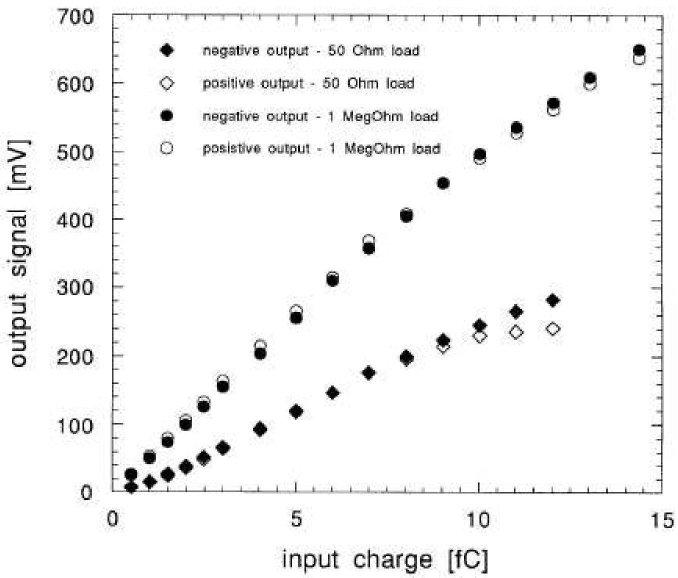

Figure 6.3: Linearity of the preamplifier for the negative and positive outputs [8].

110 ADC counts correspond to 150 mV output from preamplifier. Number of ADC counts vs. the input charge are plotted in Fig. 6.4.

AMBRA circuit is a multi-event buffer, the data comming from PASCAL are written in one of the four digital buffers of AMBRA which derandomizes the events. AMBRA also implements a 10-bit to 8-bit data compression.

The data from the four AMBRAs of each half detector are transferred at 40 MHz to the end-ladder modules. The third ASIC (CARLOS) performs the zero-supression and the compression of the data before their transmission to the DAQ system.

All three ASICs, PASCAL, AMBRA and CARLOS are implemented in a commercial 0.25 μm CMOS technology.

6.1 Simulation of the detector artefacts

The purpose is to compose the program for imitation of operation of the PASCAL circuit — amplifier, shaper and A/D converter. This problem solves program *pascal*.

For utilize information about gain 27 mV/fC is calculated total charge Q

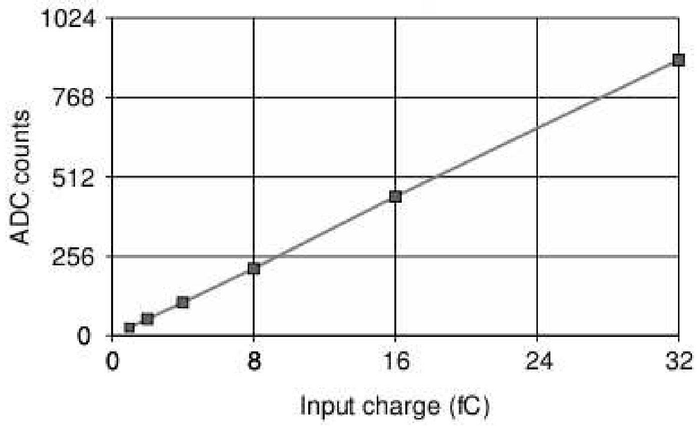

Figure 6.4: Linear dynamic range of the ADC [9].

of the input pulse $I(t)$:

$$Q = \sum_{t_{min}}^{t_{max}} I(t_n)\mathrm{d}t, \qquad (6.1)$$

where $t_{max} - t_{min}$ is time duration of the input pulse from the detector and dt is the same time step as in the detector simulation. Amplitude if the output pulse is consequently calculated as multiplication of the gain and total pulse Q.

Shaping function and noise of the preamplifier are included in frequency domain, when the input pulse $I(t)$ is transformed into frequency spectrum, where maximal frequency is given by time step and for 0.1 ns equals 5 GHz. To each frequency f_n in frequency spectrum corresponds an complex spectral amplitude $H(f_n)$ [6], [7].

Noise of the anode and of the amplifier is added into original signal in frequency spectrum as an additive component to spectral amplitudes $H(f_n)$ with constant amplitude A and uniform random phase φ with values from 0 to 2π:

$$N = A(\cos\varphi + i\sin\varphi). \qquad (6.2)$$

Peaking time of amplifier (here 40 ns) gives information of shaping function of amplifier. It is the gaussian with zero mean and $3\sigma = 40^{-1}$ ns:

$$S(f) = \frac{1}{\sqrt{2\pi\sigma^2}} e^{-\frac{f^2}{2\sigma^2}}. \qquad (6.3)$$

Response of the amplifier to input signal is given by multiplying the spectral amplitudes by shaping function: $H(f_n) = H(f_n)S(f_n)$, and taking the inverse Fast Fourier Transform to obtain signal in time reprezentation.

Finally must be the output of the inverse FFT multiplied by the constant for obtain correct pulse amplitude given by the gain of the amplifier.

The voltage curve as a response of the amplifier to the input current generated by 20 000 respective 100 000 electrons drifting from 2700 μm above detector anode edge is shown on the figure 6.5 respective 6.6.

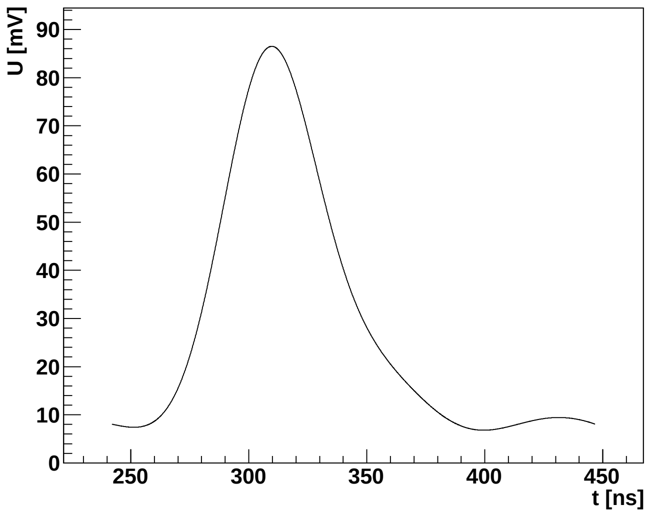

Figure 6.5: Amplifier response on input pulse of 20 000 electrons.

After preamplification the signal is sampled every 25 ns. Sampling of the preamplifier outputs from figures 6.5 and 6.6 is displayed on the figures 6.7 and 6.8.

Output voltage of the amplifier for the double hit on the detector with generation of 20 000 electrons in $y = 2000$ μm and 2500 μm (electron-holes trajectories are on the fig. 5.11 and anode current on the fig. 5.12) is on the figure 6.9 and respective ADC response on figure 6.10.

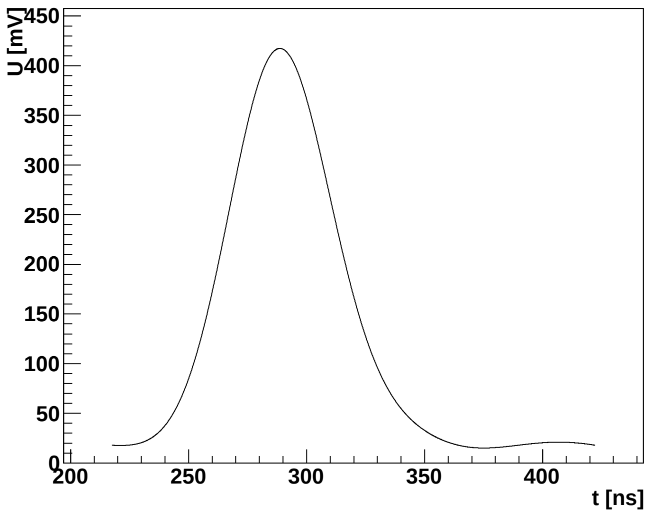

Figure 6.6: Amplifier response on input pulse of 100 000 electrons.

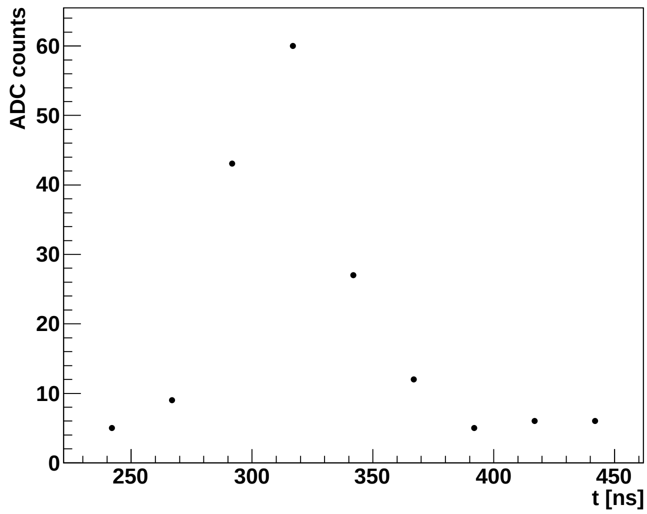

Figure 6.7: A/D converter response to the input pulse of 20 000 electrons.

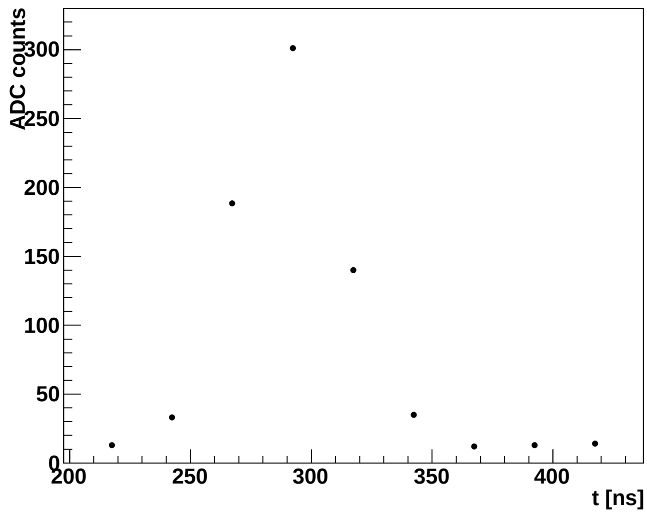

Figure 6.8: A/D converter response to the input pulse of 100 000 electrons.

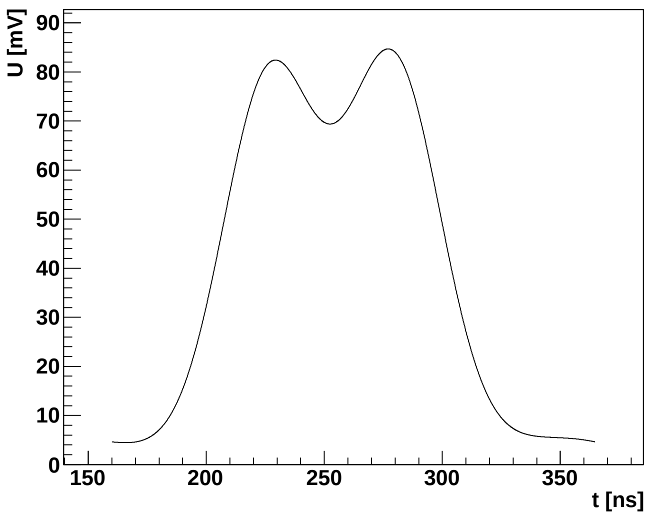

Figure 6.9: Amplifier response to the input double pulse of 20 000 electrons.

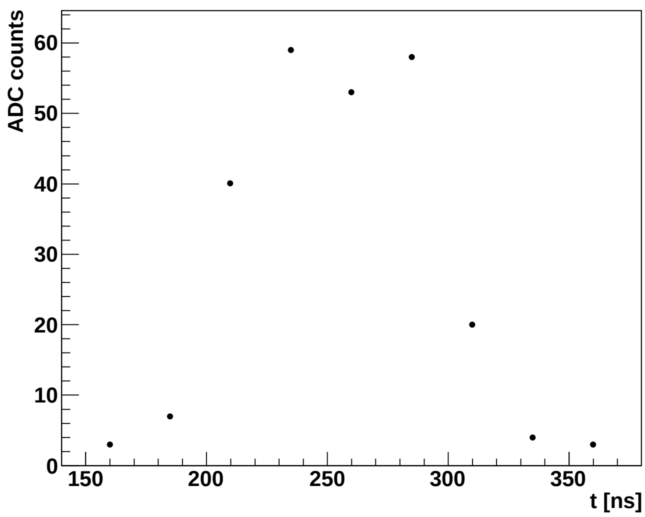

Figure 6.10: A/D converter response to the input double pulse of 20 000 electrons.

Chapter 7

The defect in the potencial of the drift electric field

7.1 Short circuit on the both sides of the detector

Possible defect in the SDD is short cicruit between several neighboring drift cathodes (all shorted cathodes are on the same voltage level). The potencial is in consequence of this deffect modified and causes differences of the drift time.

The potencial of the drift electric field with short circuit between three neighboring drift cathodes in area between y = 4350 μm and 4590 μm is drawn on the figure 7.1.

The dependence of the drift time on drift length is shown on the fig. 7.2. In the unbroken detector is this depencence linear (black), but in detector with deffect of the drift potencial (fig. 7.1) is evident the shortening of the drift time (red).

7.2 Short cicruit on the one side of the detector

Similar simulation to the previous section can be realized in the detector, which electrical potential is broken only on the one side. Such potential with five shorted drift cathodes in area between y = 2090 μm and 2420 μm on boundary with x = 300 μm is drawn on the Fig. 7.3, trajectories of the 40 000 electrons drifting throw the broken area from y = 3 000 μm are indicated on Fig. 7.4. The electrons are in broken area shifted from the middle plane

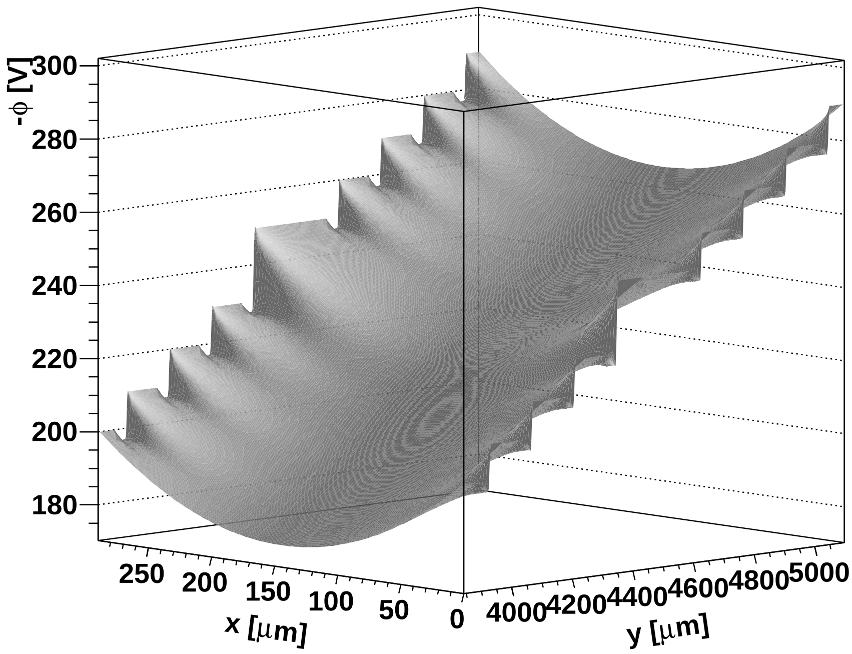

Figure 7.1: Potential of the drift electric field distorded on both sides of the detector.

of the detector towards the opposite boundary of the shorted drift cathodes.

The drift time respective for drift distances above the short cicruit are slightly higher then times for unbroken detector, but time of drift of electrons created on the bottom end of the broken area is lower due to higher local gradient of the electric potencial (Fig. 7.5).

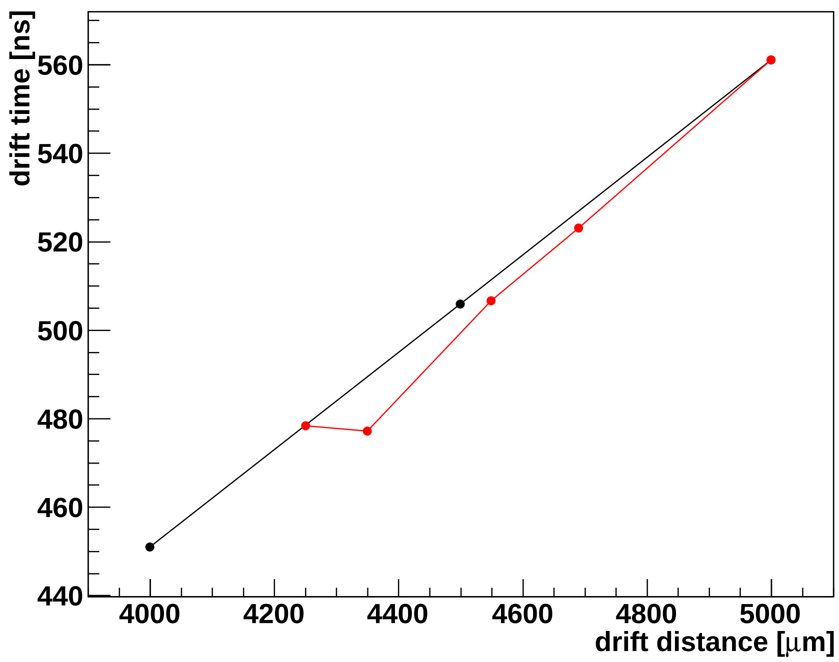

Figure 7.2: Comparison of the dependence of drift time on drift length in unbroken detector (black) and detector with short circuit on both sides — fig. 7.1 (red).

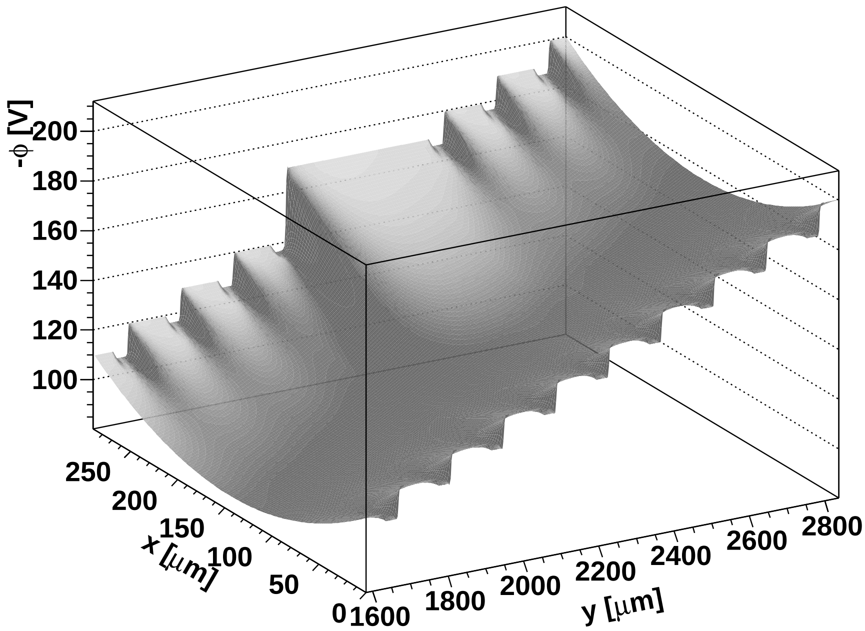

Figure 7.3: Potential of the drift electric field distorded on one side of the detector.

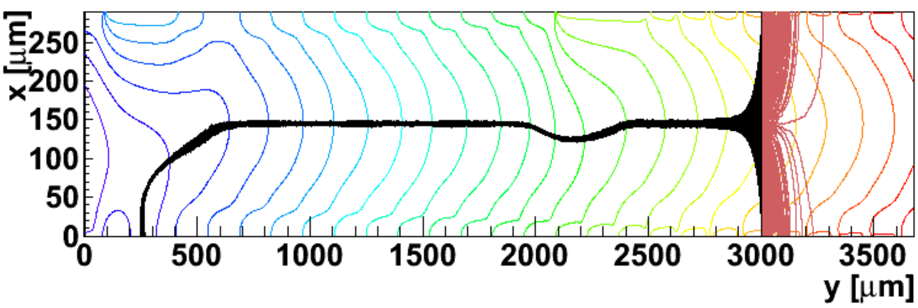

Figure 7.4: 2D projection of the paths of the 40 000 electrons (black) and holes (red) in SDD with broken potential of the drift electric field.

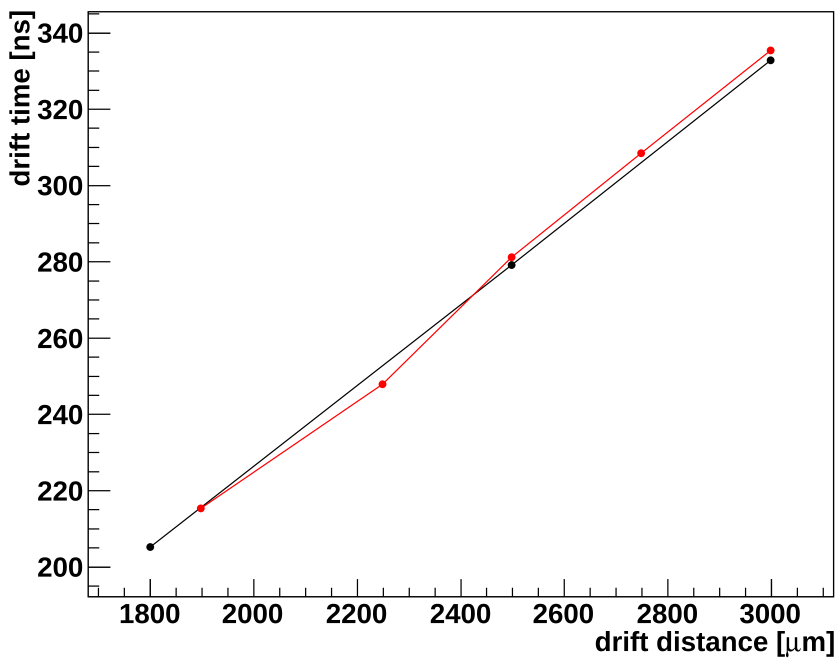

Figure 7.5: Comparison of the dependence of drift time on drift length in unbroken detector (black) and detector with short circuit on the one side — Fig. 7.3 (red).

Chapter 8

Conclusions

The purpose of project has been to compose simulation software for ALICE Silicon Drift Detectors, which allows to simulate the Silicon Drift Detector functionality since the ionizing impact until the analog-digital converter in readout electronics and includes the possibility of simultaneous multi - hits in the drift or anode direction.

The problem has been separated into two program, both written in Fortran 90, which the first, *alidrift*, simulates the carrier transport in the detector and second, *pascal*, provides simulation of the readout electronics.

Input of the *alidrift* program are three spatial hits coordinates and number of electron-holes pairs created by each ionization. Output are ascii files containing information of electrons and holes trajectories, potential of the electrical field in the simulated area and time and anode distribution of the electrons arriving into anodes. Such outputs can be visualized in the ROOT environment.

The program *pascal* takes as an input the electrical current generated in the detector anode by arriving electrons and simulates the amplifying and shaping function of the preamplifier and quantization of the preamplified signal in analog - digital converter. Outputs of the *pascal* program are voltage-like signal on the output of preamplifier and analog - digital converter counts in respective times. This simulations shows substantial extension of the input signal in time direction, which limits the resolution of the detector in drift direction.

Last chapter deals with simulations of the electrons transport in the Silicon Drift Detector throw the area with distorded potential of electrical field and analyses the consequences of the defects to dependence of drift time on drift length.

Defect of the potential is caused by short circuit of drift cathodes on the opposite sides of the detector or on the single side only. In the case of opposite shorts are drift times in affected regions lower then in good detector, in the case of single side short are drift times above the deffect slightly higher but drift times of area exactly under the defective area are lower, cause is the higher potential of the electric field.

Described detector simulator is a slow simulator, which will be used for parametrization of the ALICE SDD front-end electronics response to various situations, and these parametrizations will be used for the improvement of the fast detector simulator for ALICE SDD software.

Bibliography

[1] ALICE Collaboration, CERN/LHCC 99-12, 1999.

[2] D. Nouais, et al., Nucl. Instr. and Meth. A 501 (2003) 119 - 125.

[3] P. Rehak, et al., Nucl. Instr. and Meth. A 248 (1986) 367 - 378.

[4] E. Gatti, et al., Nucl. Instr. and Meth. A 253 (1987) 393 - 399.

[5] B. Van Zeghbroeck, Principles of Semiconductor Devices (2004).

[6] W. H. Press, et al., Numerical Recipes in Fortran 77 (1986).

[7] W. H. Press, et al., Numerical Recipes in Fortran 90 (1996).

[8] W. Dabrowski, et al., Nucl. Instr. and Meth. A 420 (1999) 270 - 278.

[9] A. Rivetti, et al., Nucl. Instr. and Meth. A 485 (2002) 188 - 192.